Synergic Identification of Prestress Force and Moving Load on Prestressed Concrete Beam Based on Virtual Distortion Method

Ziru. Xiang*[1], Tommy H. T Chan[1a], David P. Thambiratnam[1b] and Theanh Nguyen[1c]

[1]*School of Civil Engineering and Built Environment, Queensland University of Technology, 2 George St, Brisbane, Queensland 4000, Australia.*

Abstract. In a prestressed concrete bridge, the magnitude of the prestress force (PF) decreases with time. This unexpected loss can cause failure of a bridge which makes prestress force identification (PFI) critical to evaluate bridge safety. However, it has been difficult to identify the PF non-destructively. Although some research has shown the feasibility of vibration based methods in PFI, the requirement of having a determinate exciting force in these methods hinders applications onto in-service bridges. Ideally, it will be efficient if the normal traffic could be treated as an excitation, but the load caused by vehicles is difficult to measure. Hence it prompts the need to investigate whether PF and moving load could be identified together. This paper presents a synergic identification method to determine PF and moving load applied on a simply supported prestressed concrete beam via the dynamic responses caused by this unknown moving load. This method consists three parts: (i) the PF is transformed into an external pseudo-load localized in each beam element via Virtual Distortion Method (VDM); (ii) then these pseudo-loads are identified simultaneously with the moving load via Duhamel Integral; (iii) the time consuming problem during the inversion of Duhamel Integral is overcome by the load-shape function (LSF). The method is examined against different cases of PFs, vehicle speeds and noise levels by means of simulations. Results show that this method attains a good degree of accuracy and efficiency, as well as robustness to noise.

Keywords: Prestress Force Identification (PFI), Moving Load Identification, Structural Health Monitoring (SHM), Synergic Identification, Virtual Distortion Method (VDM)

1. Introduction

Prestressed concrete bridges (PCBs) have become a preferred type in bridge construction globally, for reasons of economy and savings in life-cycle costs. However, several bridge failures

*Corresponding author, Ph.D. Student, E-mail: ziru.xiang@hdr.qut.edu.au
[a] Professor, E-mail: tommy.chan@qut.edu.au
[b] Professor, E-mail: d.thambiratnam@qut.edu.au
[c] Doctor., E-mail: a68.nguyen@qut.edu.au

in the prestressed systems have caused large losses such as the collapse of Koror-Babeldaob Bridge Burgoyne and Scantlebury (2006) that killed two people and cost more than $5.2 million loss. It is necessary to develop an effective method to evaluate the existing prestress force (PF) in such bridges, not only to ensure the structural and operational safety, but also to warn of unexpected hazards.

Prestressed concrete is defined as concrete in which internal stress is introduced to counteract the stresses resulting from external load to a desired degree (Kim et al., 2003). The given external loading, which is called PF, is one of the most important parameters to control crack formation in concrete, reduce deflection and add strength to the prestressed members to reduce concrete tensile stress. As a result of elastic shortening, creep and shrinking of concrete, steel relaxation and frictional loss between tendon and concrete, prestressed concrete may lose its PF which in turn would lead to catastrophic failures of the prestressed concrete bridge. The significance of prestress force identification (PFI) is therefore obvious. However, existing PF cannot be estimated directly unless a detecting system has been instrumented at the time of construction (Lu and Law, 2006). Indirect identification methods based on vibration test data have been used and applications have been increasing since the introduction in the middle of 1990s. A critical review of representative papers is provided below.

Early researchers attempted to detect PF directly via modal characteristics such as natural frequencies of PCBs, but the implementation was found to be very difficult and sometimes almost impossible (Abraham et al., 1995). Some later studies showed that the relationship between PF and natural frequencies were subject to divided opinion. Miyamoto et al. established a natural frequency equation of a girder subjected to an external prestressed tendon and showed that the natural frequency decreases because of the dominance of the axial PF (Miyamoto et al., 2000). However, Materazzi et al. argued that in prestressed concrete beams, bonded tendons provided an increase in frequencies of the bending vibration modes, leaving the torsional modes almost unaffected (Materazzi et al., 2009). In another study, Saiidi et al. inferred that the practical range of PF has little influence on the natural frequencies of prestressed concrete members (Saiidi et al., 1994). Most of the previous results indicate the difficulties of PFI via modal characteristics as being: 1) almost impossible to identify PF through the natural frequencies because they are not sensitive to the PF change and vary conversely between different prestressing technologies (pre-tension and post-tension, bonded and unbonded tendons); 2) difficult to identify PF from the measured mode shapes because they remain almost identical under different PFs.

More recently, some methods to assess PF inversely were derived using dynamic responses like strains or accelerations measured from forced vibration tests. However, lack in accuracy, stability and utility of these methods hampered real applications. Law and Lu (2005) stated it is feasible to measure PF through strain or displacement excited by an impulse force with or without the flexural rigidity of the beam. Later, they proposed a model updating method to assess the PF and conducted a laboratory experimental validation, however, the results were shown to be sensitive to the combination of the model error and measurement noise (Lu and Law, 2006). These studies only simply considered the PF as a compressing force to be applied in the centroid of the beam cross section, while in practical cases prestressing tendons are often eccentric. Xu and Sun (2011) found that the effect of eccentricity is an important factor that affects the accuracy of PFI. A velocity-response-sensitivity based method was proposed in their research and the eccentricity of prestressing tendon was considered. However, numerical results showed up to 21% error which would be excessive for practical applications. Recently, Li et al. (2013) established a strain-displacement relationship of a plate shell element to identify the PF in a box girder bridge model.

They conducted a model updating study via measured responses from moving vehicle loads, but large error was observed under a weak road condition.

The above paper review highlights that most of existing vibration based methods require a known exciting force which in practice is inconvenient because bridges need to be closed during testing, or passing vehicles may affect the excitation. In fact, the ideal excitation for in-service bridges is the traffic loads, but these loads are usually difficult to measure. The methods used in the prior studies were either based on given external excitation (Law and Lu, 2005, Lu and Law, 2006, Xu and Sun, 2011), or required a known moving force (Li et al., 2013), which means the application of these methods to actual structures may still have some difficulty. Nevertheless, it can be seen that vibration based methods have a great potential for use in PFI. At the same time, there has been plenty of room left for improvement such as detection of the PF under an unknown moving load or implementation of the methods under demanding operating conditions of in-service structures. In this paper, a synergic identification method will be developed to determine the PF in a prestressed beam using its dynamic responses due to an unknown moving load.

2. Synergic Identification Method

This section presents a synergic identification method to identify the moving load and PF in a simply supported beam. The proposed method is the combination of three methods: Virtual Distortion Method (VDM) is used to transform PF into an external pseudo-load so that the identification of PF and moving load will become a multi-force identification of a pseudo-load and a moving load; Duhamel integral is used to determine these loads; and the load-shape function (LSF) will be introduced to improve the computing efficiency and overcome the ill-condition problem (Wang et al., 2012).

2.1 Virtual distortion method (VDM)

VDM is a quick reanalysis method applicable for statics and dynamics of structures which has been used in structural damage identification (Kołakowski et al., 2008). The variations in structure (including structural damage) are modelled in forms of the related responses-coupled virtual distortions imposed on the original (undamaged) structure. Once the original structure is modelled, all the upcoming structural variations can be simulated as added virtual distortions, instead of remodeling the whole structure. Because of its merit, VDM is employed in this research to facilitate the modeling process.

Based on VDM, PF is modelled as an equivalent pseudo-load. Thus the prestressed structure is modelled by a non-prestressed structure (called as an original structure here) subjected to the pseudo-load. This pseudo-load is related to the PF and the structural dynamic response. Hence based on the principle of superposition, the response of the prestressed structure due to an external excitation can be expressed as a sum of the responses of the original structure due to the same excitation and the pseudo-load. In this way, the response of the prestressed structure can be expressed solely in terms of certain characteristics of the original structure.

As Fig. 1 shows, a simply supported prestressed concrete beam with an internal prestressed tendon is established. The PF is applied through the prestressing tendon. With a moving force applied along the beam, the equation of motion of the prestressed beam can be written as

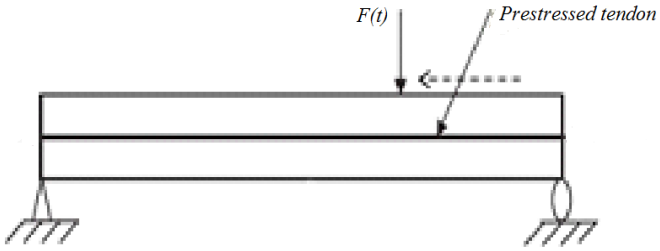

Fig. 1 A simply supported prestressed beam

$$[M]\{\ddot{x}\}+[C]\{\dot{x}\}+[\overline{K}]\{x\}=[B]f(t) \tag{1}$$

$$\overline{K}=K-K_g \tag{2}$$

where x, $\dot{x}$ and $\ddot{x}$ are the displacement, velocity and acceleration vectors, respectively; M, C and $\overline{K}$ are the mass, damping and global stiffness matrix of the prestressed girder, respectively; $f(t)$ is a moving excitation force vector, while B is its mapping matrix; K is the global stiffness matrix of the beam without PF, i.e. the original structure, and K_g is the stiffness matrix contributed by PF which is named as global geometrical stiffness matrix (Lu and Law, 2006).

Assuming Rayleigh damping is used, damping matrix can therefore be represented by a linear combination of the system mass and stiffness matrices,

$$C=\alpha[M]+\beta[\overline{K}] \tag{3}$$

Where α and β are the Rayleigh damping coefficients.

Eq. (1) can be transformed into the equation of motion of the original structure subjected to the same external excitation $f(t)$ and a response-coupled pseudo-load $\{P\}$

$$[M]\{\ddot{x}\}+[C]\{\dot{x}\}+[K]\{x\}=[B]\{F\}+\{P\} \tag{4}$$

$$\{P\}=[K_g]\{x\} \tag{5}$$

where $\{P\}$ models the influence of PF and is related to the global geometrical stiffness matrix and the displacement response, which is a time dependent function.

The synergic identification of moving load and PF therefore turns into the identification of the moving load and the pseudo-load.

The global geometrical stiffness matrix K_g can be expressed as

$$[K_g]=\sum_{1}^{N}L_i^T R_i^T K_{g,i}^e R_i L_i \tag{6}$$

N is the total number of the elements. L_i, R_i and $K_{g,i}^e$ are the mapping, transformation and local geometrical stiffness matrices of the i^{th} element, respectively. $K_{g,i}^e$ can be written as (Lu and Law, 2006)

$$K_{g,i}^{e}=\frac{T}{30\eta}\begin{bmatrix}30 & 0 & 0 & -30 & 0 & 0\\ 0 & 36 & 3\eta & 0 & -36 & 3\eta\\ 0 & 3\eta & 4\eta^{2} & 0 & -3\eta & -\eta^{2}\\ -30 & 0 & 0 & 30 & 0 & 0\\ 0 & -36 & -3\eta & 0 & 36 & -3\eta\\ 0 & 3\eta & -\eta^{2} & 0 & -3\eta & 4\eta^{2}\end{bmatrix} \qquad i=1,2,3,....,N \tag{7}$$

where T is the magnitude of PF, η is the length of the element.

The nodal displacement of i^{th} element in the local coordinate can be written as

$$\{x\}_i^e = R_i L_i \{x\} \tag{8}$$

Substituting Eqs. (6) and (8) to Eq. (5) leads to presentation of the pseudo-load via local nodal displacements as reflected through Eqs. (9) and (10) as follow

$$\{P\}=\sum_{i}^{N} L_i^T R_i^T \{P\}_i^e \tag{9}$$

where $\{P\}_i^e$ is the local pseudo-load of the i^{th} element,

$$\{P\}_i^e = K_{g,i}^e \{x\}_i^e = \frac{T}{30\eta}\begin{bmatrix}30 & 0 & 0 & -30 & 0 & 0\\ 0 & 36 & 3\eta & 0 & -36 & 3\eta\\ 0 & 3\eta & 4\eta^{2} & 0 & -3\eta & -\eta^{2}\\ -30 & 0 & 0 & 30 & 0 & 0\\ 0 & -36 & -3\eta & 0 & 36 & -3\eta\\ 0 & 3\eta & -\eta^{2} & 0 & -3\eta & 4\eta^{2}\end{bmatrix}\{x\}_i^e \tag{10}$$

We should mention that $\{x\}_i^e$ is the displacement of the real structure of interest (with PF), which can be measured directly. Thus, as long as $\{P\}_i^e$ is identified, the PF value of T can be calculated.

In VDM, the local pseudo-load modifies the element in the form of virtual forces. And all these forces follow the modified element's own vibrational behavior, which means the virtual forces will act exactly the same way as the nodal forces of the element. For example, a two-dimensional beam element has three components of its nodal forces: axial force, shear force and bending moment, which are caused by three states of deformation: axial compression or tension, pure bending and bending plus shearing. Then the local pseudo-load can be written as a combination of its virtual forces:

$$\{P\}_i^e = \sum_k p_{ik}(t) \tag{11}$$

where $p_{ik}(t)$ is the k^{th} virtual force caused by the i^{th} local pseudo-load.

2.2 Duhamel integral implementation based on LSF

With the assumption of zero initial conditions, the dynamic response is obtained by the convolution of all external forces and their impulse response functions. As the internal prestress force has been transformed to external virtual force $p_{ik}(t)$, the responses are obtained by Duhamel integral of both $f(t)$ and $p_{ik}(t)$:

$$y_j(t) = \int_0^t h^j(t-\tau) f(\tau) d\tau + \sum_i^N \sum_k \int_0^t d_{ik}^j(t-\tau) p_{ik}(\tau) d\tau \qquad j = 1,2,3... \tag{12}$$

where $y_j(t)$ is the j^{th} measured response; $h^j(t-\tau)$ is the j^{th} impulse response function between j^{th} sensor and $f(t)$ on original structure; $d_{ik}^j(t-\tau)$ is the impulse response function between j^{th} sensor and $p_{ik}(t)$ on the original structure, and in the scope of VDM it is called the dynamic influence function.

Practically, responses measured by sensors are discrete. The matrix form of Eq. (12) is usually used. Given a certain time period, the convolution can be approximated by the product of external force matrix and its impulse response function matrix:

$$Y_j = H^j F + \sum_k \sum_i^N D_{ik}{}^j P_{ik} \qquad j = 1,2,3... \tag{13}$$

where Y_j is the discrete response measured by j^{th} sensor. F and P_{ik} are the discrete moving load and virtual force vector respectively. H^j and $D_{ik}{}^j$ are matrixes composed by impulse response functions between the j^{th} sensor and F and P_{ik} respectively.

To ensure the uniqueness of the solution of linear system Eq. (13), the number of test points (responses) is required not less than the number of unknown external loads. Thus in practice, the number of unknowns should be predicted in order to estimate the number of sensors. Since the number of virtual forces is related to the element division of structure, a proper FE model is necessary before testing.

The system matrices in Eq. (13) can be large and difficult to compute in the cases of long sampling duration or dense time discretization. Also, in majority of practical cases, this matrix is ill-conditioned, which means a small disturbance in measured response can cause a large error in the identified results. Typical regularization solutions for the ill-conditioned problem are the truncated singular value decomposition (TSVD) and Tikhonov method (Jacquelin et al., 2003). However, these methods require heavy computational efforts. In this paper, the author intends to introduce LSF to overcome these drawbacks as LSF can not only manage the ill-conditioned problem but also boost the calculation efficiency.

The idea of LSF is analogous to the shape function in FEM. It formulates the discrete time history of unknown force as a 'beam', and then the variation of force can be simulated based on 'vertical displacements' and 'rotations' of a limited set of evenly distributed 'nodes'.

In FEM, the shape function of a beam element can be written as:

$$n = \left[1 - 3\xi^2 + 2\xi^3, \xi - \xi^3, 3\xi^2 - 2\xi^3, \xi^3 - \xi^2\right] \tag{14}$$

Assuming $\xi = 0:1/l:1$, where l denotes the time step between each 'node', leads to the LSF matrix reflected through Eq. (15) (Zhang, 2010)

$$n = \begin{bmatrix} 1 & 0 & 0 & 0 \\ 1-3(1/l)^2+2(1/l)^3 & (1/l)[1-(1/l)^2] & (1/l)^2[3-2(1/l)] & -(1/l)^2[1-(1/l)] \\ 1-3(2/l)^2+2(2/l)^3 & (2/l)[1-(2/l)^2] & (2/l)^2[3-2(2/l)] & -(2/l)^2[1-(2/l)] \\ \cdots & \cdots & \cdots & \cdots \\ 0 & 0 & 1 & 0 \end{bmatrix} \tag{15}$$

If we define the time between each node as half of the period of LSF, then the frequency of LSF f_{LSF} will be

$$f_{LSF} = f_s / 2l \tag{16}$$

where f_s is the sampling rate.

The frequency of LSF is required higher than the main range of frequency of the unknown force in order to simulate all its details (Zhang et al., 2008). For an unknown force, its frequency distribution can be determined by the Fourier transformation of measured response. Thus, the specification of f_{LSF} can be determined by the spectral analysis of measured response. Assuming ω is the highest frequency of interest of the unknown force, which will be considered as the referenced frequency of LSF, the time step between each node shall be determined:

$$l = f_s / 2\omega \tag{17}$$

And if the time duration of the unknown force is *Z,* the total time step of the duration ('beam') will be Zf_s; thus the number of 'node' can be determined as $\frac{Zf_s}{l}+1$. As each node has two LSFs, the number of LSF will be

$$m = 2(\frac{Zf_s}{l}+1) \tag{18}$$

Therefore, the unknown force is represented by the LSF and its corresponding coefficients in the same way as using the shape function to present the beam deformations.

$$F = N\alpha \tag{19}$$

Where N is the matrix which collects the LSF matrices of all the 'beam' elements, α is its coefficient vector.

The coefficient α, which is much smaller in dimension than F, is now to be identified instead of F. Therefore, the computational effort is reduced (which will be described in detail in 3.2). In addition, because the estimated load is smoothed via LSF to some degree, the influence of noise will be minimized even without regularization (Zhang et al., 2008).

The virtual forces can be regarded as a time consequent force which is able to apply LSF as well. By comparing Eq. (13) with Eq. (19), the LSF equation for Duhamel integral is:

$$Y_j = H^j N\alpha_F + \sum_k \sum_i^N D_{ik}^j N\alpha_{ik} = B_F^j \alpha_F + \sum_k \sum_i^N B_{ik}^j \alpha_{ik} \tag{20}$$

$$B_F^j = H^j N \tag{21}$$

$$B_{ik}^j = D_{ik}^j N \tag{22}$$

α_F is the relevant coefficient of the moving load and α_{ik} is the coefficient for the k^{th} virtual force caused by the i^{th} local pseudo-load. There should be at least as many independent responses as the total number of unknown coefficients to guarantee the uniqueness of the solution, so the number of sensors should be no less than $kN+1$.

$$\begin{bmatrix} \alpha_F \\ \alpha_{11} \\ : \\ : \\ \alpha_{kN} \end{bmatrix} = \begin{bmatrix} B_F^1 & B_{11}^1 & .. & .. & B_{kN}^1 \\ : & : & & & \\ : & & : & & \\ : & & & : & \\ B_{kN}^{kN+1} & & & & B_{kN}^{kN+1} \end{bmatrix}^+ \begin{bmatrix} Y_1 \\ Y_2 \\ : \\ : \\ Y_{kN+1} \end{bmatrix} \tag{23}$$

In this paper, as the beam is excited by a moving (vertical) load, it is assumed that no axial force is present in beam elements. Thus there are only 2 types of virtual forces (bending moment and shearing force), or *k=2*. Then, the moving load and virtual force can be determined through:

$$F = N\alpha_F \tag{24}$$

$$P_{ik} = N\alpha_{ik} \tag{25}$$

3. Case Studies

3.1 The prestressed beam details

A 20m long simply supported prestressed concrete beam is established. The second moment of area of concrete cross section is 0.372 m^4 while the tendon cross section area is 1.39×10^{-4} m^2. The Young's modulus of the beam and the tendon are 3.45×10^{10} N/m^2 and 2.95×10^{11} N/m^2, the densities are 2.3×10^3 kg/m^3 and 7.9×10^3 kg/m^3, and the Poisson's ratios are 0.2 and 0.3, respectively.

The magnitude of PF is designed according AASHTO (AASHTO, 1998). In order to simplify the simulation, PF is applied at the centroid of the beam's cross section and a uniform compressive stress will be introduced across its entire depth without any eccentricity. For post-tensioned concrete component, the strength-capacity reduction factor is taken as 0.95. Thus, the practical range of PF is designed as 850 – 1220 KN. The exciting force is chosen as a time-varying moving load $f(t) = 2[30 + 2\sin(10\pi t) + 4\cos(15\pi t) + \cos(3\pi t + 0.2\pi)]$ (KN).

This simulation is conducted using ANSYS software. Elements solid186 and link8 are chosen to simulate the concrete and tendon respectively. The beam is divided into 10 elements. Thus, the unknowns are 1 moving load and 20 virtual forces (one bending moment and one shear force in each element). The translational and rotational responses of each node are measured which means 20 sensors are needed to place along the beam. Fig. 2 shows the sensor placement (at both ends, only rotational motions are needed to measure). Rayleigh damping is applied according to Eq. (3) and the sampling rate is taken at 200Hz.

x: sensor to measure translation responses
+: sensor to measure rotational responses
o: node

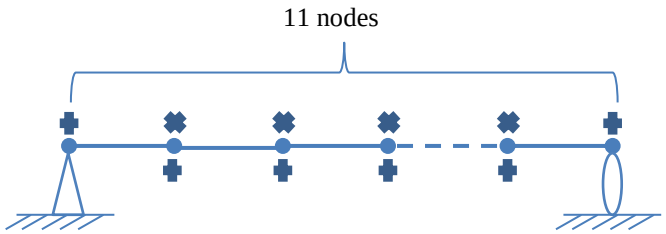

Fig. 2 Sensor placement

3.2 Case setting

As road surface roughness as well as measurement noise may affect the identification (Li et al., 2013), different levels of white noise are considered in the case study in order to account for the adverse road condition and measurement uncertainties,

$$Y^n = Y \times (1 + \psi N(0,1)) \tag{26}$$

where Y^n and Y is the responses with and without noise, respectively; ψ is a relatively high amount of noise percentage; $N(0,1)$ is a matrix containing pseudorandom values drawn from the standard normal distribution.

To ensure the synergic identification method can produce good results for all traffic situations, different moving load speeds are taken into account in the case study as well. As the proposed method is aimed to use the normal traffic load as excitation, practical ranges of speeds are considered: 13.3, 22.2 and 33.3 m/s.

Therefore, the cases are set as follow:

Table 1 Case setting

Case No.	PF (KN)	Noise (%)	Speed (m/s)	Case No.	PF (KN)	Noise (%)	Speed (m/s)
1	850	0	22.2	**8**	1200	0	22.2
2	850	5	22.2	**9**	1200	5	22.2
3	850	10	22.2	**10**	1200	10	22.2
4	850	0	13.3	**11**	1200	0	13.3
5	850	10	13.3	**12**	1200	10	13.3
6	850	0	33.3	**13**	1200	0	33.3
7	850	10	33.3	**14**	1200	10	33.3

3. 3 Optimization of computation using LSF

As described earlier, the highest frequency of moving force will be taken as reference for f_{LSF}. Taking Case 1 as an example, the Fourier transformation of the mid-span displacement response is shown:

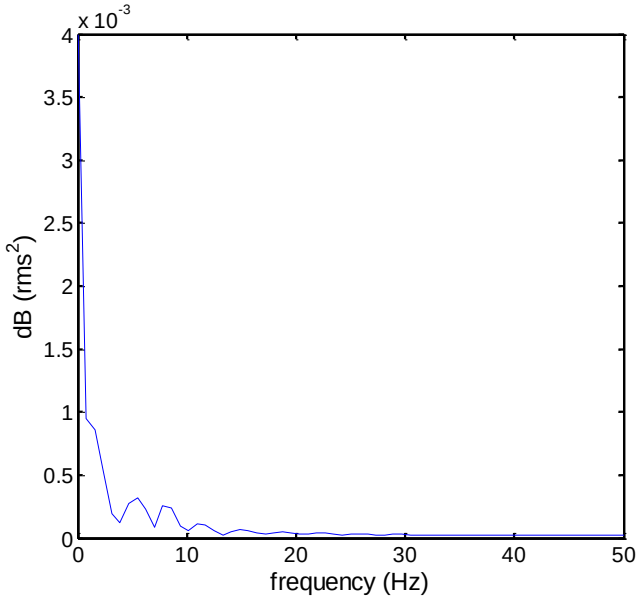

Fig. 3 Fourier transformation of mid-span displacement

It can be observed that the main range of frequencies of interest is less than 10 Hz, therefore f_{LSF} is taken as 10. According to Eqs. (17) and (18) and taking Z as 0.9s, we can obtain $l = 10$ and $m = 38$, which means 38 LSFs are applied and each function has 10 steps.

The improvement of this procedure can be revealed clearly from the decrease of the calculation. Taking Case 1 as an example: before LSF is introduced, the impulse response matrix H and dynamic influence matrix D_{ik} both have dimensions of 3600×3600 (which is calculated by the product of the total number of time step and the number of sensors). After adopted, we only need to calculate B_F and B_{ik} instead of H and D_{ik}. As the dimensions of B_F and B_{ik} are only 3600×38, the computing load of inversion has been decreased from 3600×3600^2 to 3600×38^2, which is around 9000 times faster. This shows LSF can prominently improve the computational efficiency.

3.4 Results and discussion

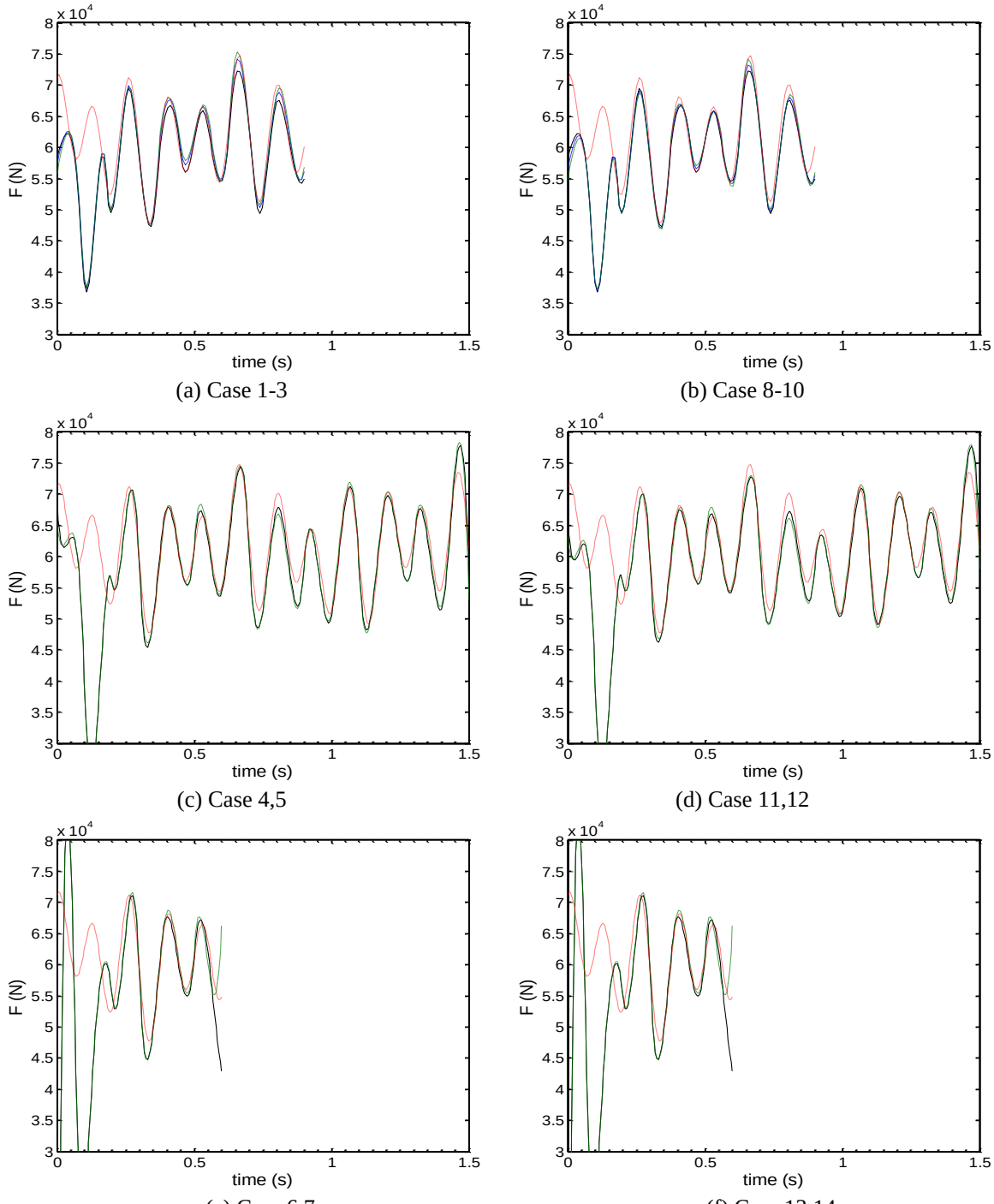

(a) Case 1-3

(b) Case 8-10

(c) Case 4,5

(d) Case 11,12

(e) Case 6,7

(f) Case 13,14

Fig. 4 Results of Moving force identification

The synergic identification results of 14 cases are compared in this section. Those results of moving load and PF are shown separately but are identified simultaneously. Influences caused by different amplitude of PF, noise and vehicle speed are analyzed from the comparison of each case.

In Fig. 4 moving load identification results are pictured. As expected, large errors are found in elements close to the start and end of the time histories which is typical in moving load identification problems (Chan et al., 2001, Law et al., 2004) due to instability of vibration responses at the beginning and end of the period. The results from elements in the middle of the beam show good agreement with the true value in both cases of original PFs. The effect of noise can mainly be seen at peak values of the load profile and generally small, which shows that LSF can enhance the robustness of the identification method against noise. Moving loads with speed of 13.3 m/s, 22.2 m/s and 33.3 m/s (which represent the ordinary traffic speeds) are all determined with a good degree of accuracy, which proves that this method is not affected by vehicle speeds and can be used in different practical situations.

Figs. 5, 6 and 7 show the PFI result of each element in the synergic identification process. The PF value of T is calculated through Eq. (10) from the local displacement response and identified pseudo-load, which makes the value of T not constant but varying with time. Fig. 5 shows full PFI results for all 10 elements. In the other figures, only 4 representative elements (3, 5, 7, and 9) are reported for the purpose of clarity.

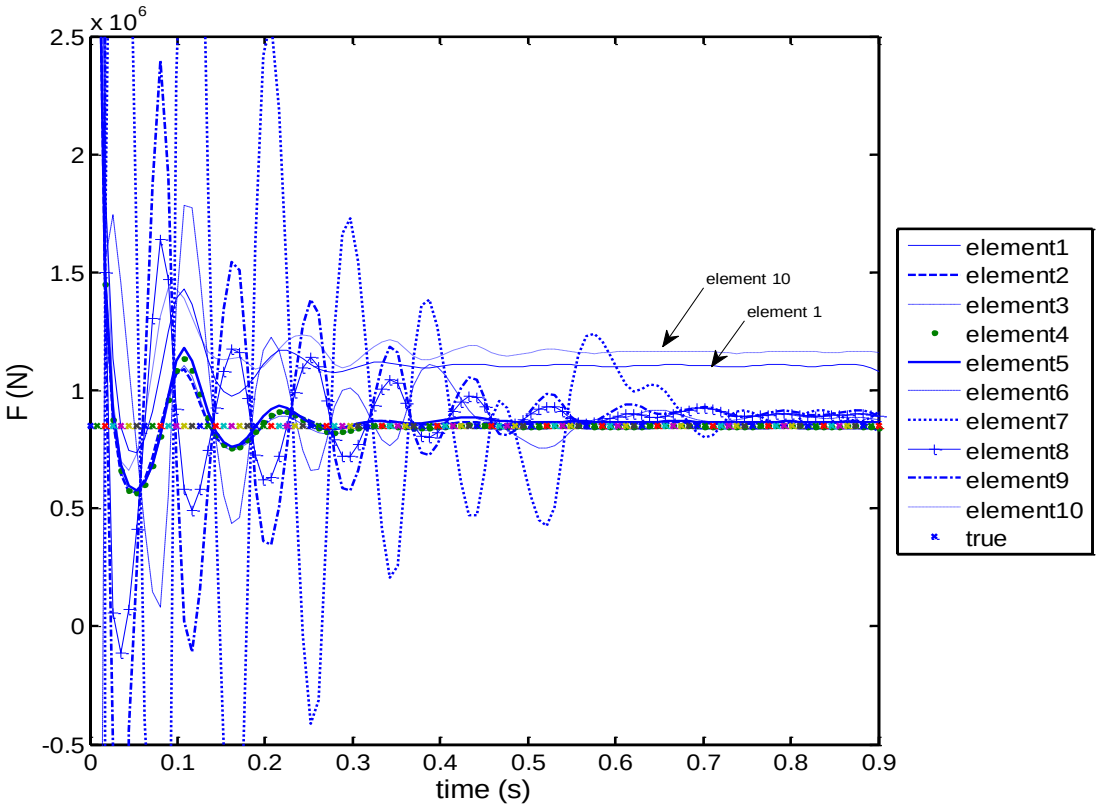

Fig. 5 Results of PFI without noise (all elements reported)

- **Identification for different PF levels**
  From Fig. 5 (the result of Case 8 is not plotted as it is very similar to Case 1), we can find the varying tendency of *T*. Firstly, it can be seen that the PF results of each element are not stable at start for a small period and then converged to a constant value approximating its true PF value. Secondly, the converged values of most elements are approximate to the true PF except for elements 1 and 10 (as marked in the figure) which are elements at the two supports. However, elements closed to mid-span such as elements 4, 5 and 6 show better results. Moreover, in Fig. 6, both PFs of 850 KN and 1200 KN are correctly estimated and clearly distinguished which mean that the method works well with different PF values in practical ranges.

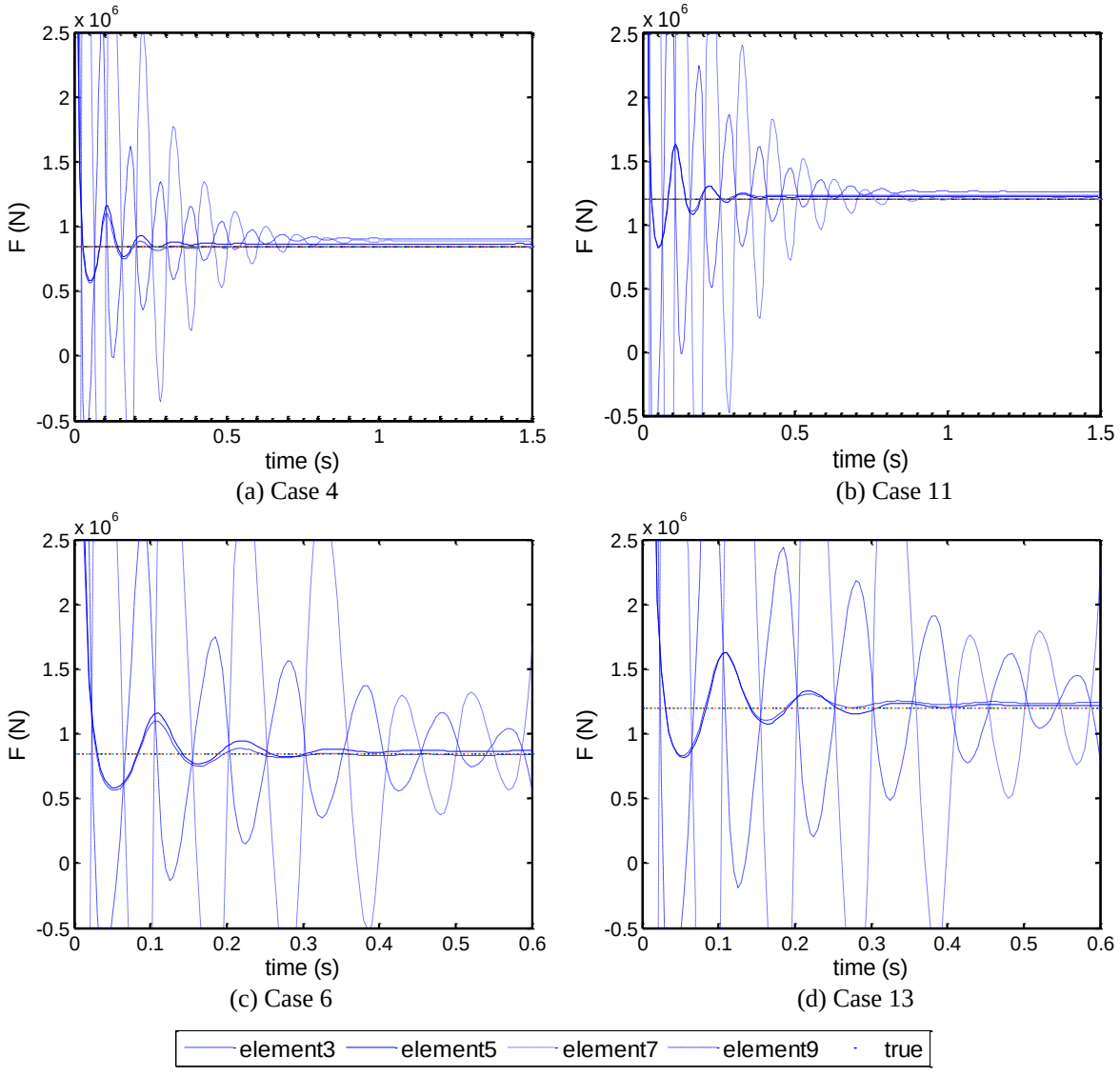

(a) Case 4 (b) Case 11

(c) Case 6 (d) Case 13

Fig. 6 Result of PFI without noise (representative elements reported)

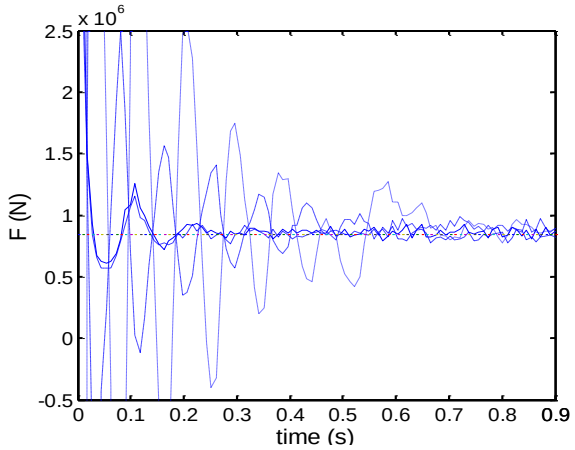

(a) Case 2

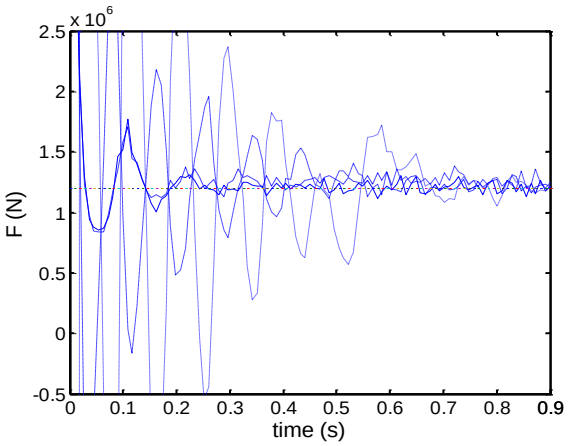

(b) Case 9

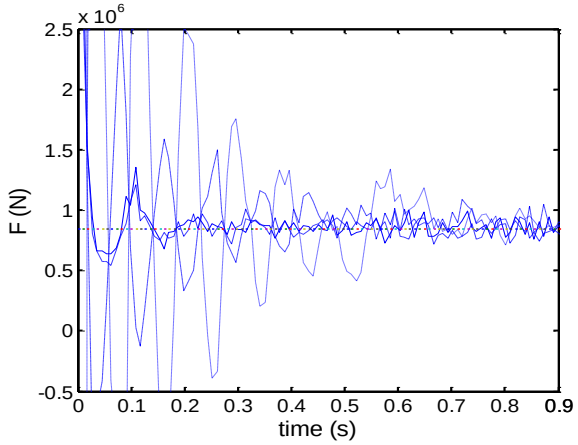

(c) Case 3

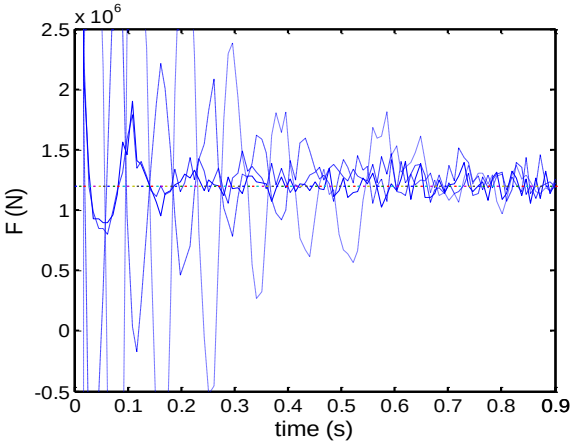

(d) Case 10

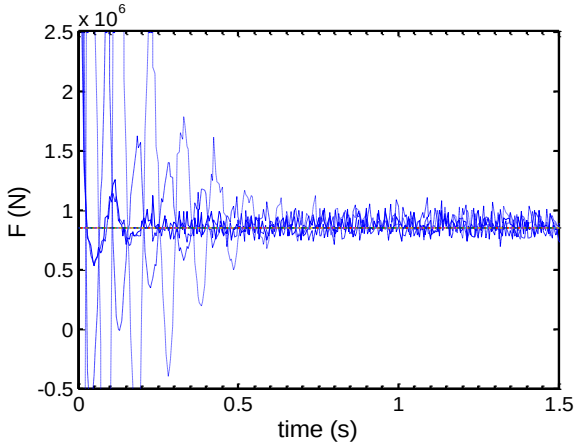

(e) Case 5

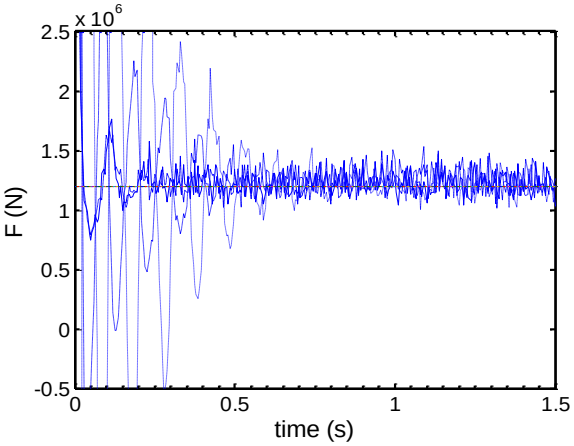

(f) Case 12

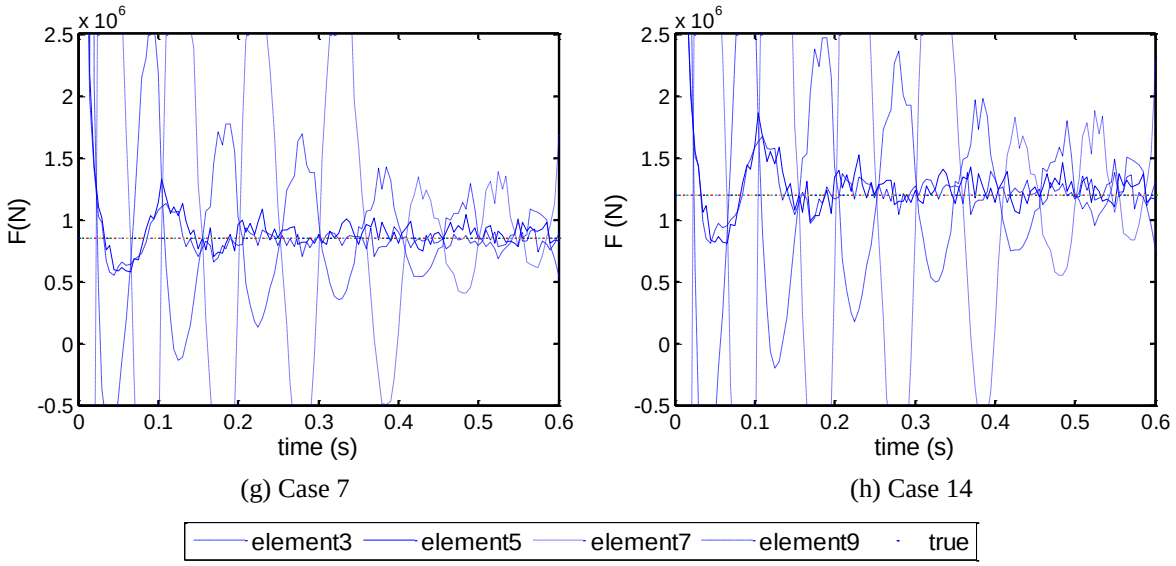

(g) Case 7 (h) Case 14

Fig. 7 Results of PFI with noise(representative elements reported)

- **Influence of vehicle speed**
  Comparing Figs. 6(a) with (c) [or (b) and (d)], we can find the elements in the beginning will have shorter converging time than the follower elements. Also, the general converging times of *T* function are consistently around 0.45-0.7s even with different speed of moving load. Therefore, it is required that the travelling time of vehicle should not be shorter than this converging time; or it may cause some trouble, as shown in Figs. 6(c) and (d) the travelling time period is only 0.6s during which elements 7 and 9 have not been able to converge and this would obviously decrease the identification accuracy. Nevertheless, this can be considered as an extreme case since the vehicle speed has reached 33.3m/s (120 km/hr) while the beam is only 20m long. In practice, prestressed beams or girders are usually much longer; this requirement will not have much impact on the application.
- **Influence of noise**
  Comparing the pictures in Fig. 7, we can find that noise has some impact on results. Although noise does increase the roughness of *T* function curves, the overall changing trend has not been much affected. This is because that LSF has minimized the impact caused by noise in during inversing process, the identification of moving load and virtual forces therefore are robust to noise. However, the noise is introduced again with the measured responses in Eq. (10) when calculating the linear solution *T*. Hence, the disturbance of noise only causes some local fluctuations in the *T* function curves and will not affect much the convergence of *T*.

Considering all the influences stated above, the following steps should be taken into account in the implementation of the method developed herein to improve the PFI accuracy: 1) Excluding the elements at boundaries (i.e. elements 1 and 10 in this case) which are associated with computational instability; 2) Taking into account the values after sufficient convergence is

accomplished, in this case is 0.45s; 3) calculating the average of selected values to obtain the final PF value (in order to reduce the influence of noise).

Table 2 Results of PFI

PF / Speed / Element	850.00 (KN)			1200.0 (KN)		
	13.3 m/s	22.2 m/s	33.3 m/s	13.3 m/s	22.2 m/s	33.3 m/s
2	853.60 - 858.14	859.20 861.62 865.57	854.01 - 863.15	1212.3 - 12187	1223.8 1223.6 1229.3	1212.9 - 1225.9
3	836.25 - 837.98	836.17 839.18 844.06	837.20 - 837.83	1227.7 - 1230.3	1238.8 1239.1 1246.8	1236.7 - 1237.6
4	847.03 - 843.47	847.36 847.16 848.73	848.09 - 832.67	1234.1 - 1229.0	1238.2 1234.2 1236.6	1235.7 - 1213.2
5	866.45 - 864.75	866.90 860.98 856.82	866.39 - 886.13	1216.4 - 1214.0	1220.7 1208.6 1202.9	1216.4 - 1244.1
6	851.60 - 855.89	867.14 860.76 856.42	939.37 - 954.12	1207.4 - 1212.8	1185.3 1172.9 1167.1	1280.1 - 1300.2
7	884.41 - 888.97	891.68 893.87 897.54	981.95 - 990.19	1203.4 - 1205.7	1212.7 1212.4 1217.3	1331.8 - 1343.0
8	896.82 896.03	894.54 899.07 905.59	879.92 - 874.61	1234.6 - 1233.5	1237.7 1240.4 1249.3	1213.9 - 1206.6
9	906.90 - 909.41	904.06 905.76 909.60	873.95 - 860.63	1260.0 - 1263.5	1264.4 1263.0 1268.5	1218.8 - 1200.2
Average	867.89 - 869.33	870.88 871.05 873.04	885.11 - 887.41	1223.9 - 1226.5	1224.1 1227.5 1227.2	1243.3 - 1246.3
Error	2.10% - 2.27%	2.46% 2.48% 2.71%	4.13% - 4.40%	1.99% - 2.17%	2.01% 2.02% 2.27%	3.61% - 3.86%

*Values in each cell are listed by 0% noise, 5% noise and 10% noise.

As a result, Table 2 shows the identified value of elements 2-9 and the error between the average and true value. The results show that the PF values of all cases are determined with good accuracy; errors are limited under 4.40%. In terms of the influence between different PFs, we can find that higher PF will lead to a better PFI result. For the effect of vehicle speed, it is shown that lower speed will produce a better result and this can be seen on the cases of 13.3 m/s and 22.2 m/s with which the error is less than 2.46%. When the vehicle speed increases to 33.3 m/s, because of

T function of some elements not being well converged in the time duration, the PFI accuracy decreases. In the cases with noise, with the optimization of the proposed procedure, we could eliminate the majority of the noise effects, especially when the noise level is only 5%, the influence can be ignored.

4. Conclusions

A synergic identification method to assess PF and moving load in a prestressed concrete beam is proposed. The PF is transformed into an external force by means of VDM and determined simultaneously with moving load accurately and efficiently through the LSF-enhanced Duhamel integral. Case studies with three parameters (PF amplitude, vehicle speed and noise level) are conducted. The moving load is identified with a great degree of accuracy in all cases with the assistance of LSF. In terms of PFI, PF is also estimated with good accuracy and stability: different amplitudes of PF in a practical range are clearly identified and the influence of noise can be overcome by the proposed optimization procedure. Results show that PF requires a certain period of time to converge and be identified, which means high vehicle speed (or short transit duration) may have some impact on the identification accuracy. Nevertheless, in most cases bias can be restricted to be fewer than 4%, which can be considered to be acceptable in practical applications. Exclusion of elements at supports and having sufficient time for convergence are found to be necessary to enhance the PFI results against uncertainties. The application of the method has shown its great potential in determining PF in beams, and further extension of the method for use with prestressed concrete box girder will be a future research topic for the authors.

References

AASHTO (1998), *Bridge Design Specifications.* American Association of State Highway and Transportation Officials, Washington, DC.

Abraham, M. A., Park, S. and Stubbs, N. (1995), "Loss of prestress prediction based on nondestructive damage location algorithms", *Smart Structures & Materials' 95*.

Burgoyne, C. and Scantlebury, R. (2006), "Why did Palau bridge collapse?", *The Structural Engineer,* **84,** 30-37.

Chan, T. H. T., Yu, L., Law, S. S. and Yung, T. H. (2001), "Moving force identification studies, I: Theory", *Journal of Sound and Vibration,* **247,** 59-76.

Jacquelin, E., Bennani, A. and Hamelin, P. (2003), "Force reconstruction: analysis and regularization of a deconvolution problem", *Journal of Sound and Vibration,* **265,** 81-107.

Kim, J.-T., Ryu, Y.-S. and Yun, C.-B. (2003), "Vibration-based method to detect prestress loss in beam-type bridges", *Smart Structures and Materials*.

Kołakowski, P., Wikło, M. and Holnicki-Szulc, J. (2008), "The virtual distortion method—a versatile reanalysis tool for structures and systems", *Structural and Multidisciplinary Optimization,* **36,** 217-234.

Law, S., Bu, J., Zhu, X. and Chan, S. (2004), "Vehicle axle loads identification using finite element method", *Engineering Structures,* **26,** 1143-1153.

Law, S. S. and Lu, Z. (2005), "Time domain responses of a prestressed beam and prestress identification", *Journal of sound and vibration*, **288,** 1011-1025.

Li, H., Lv, Z. and Liu, J. (2013), "Assessment of prestress force in bridges using structural dynamic responses under moving vehicles", *Mathematical Problems in Engineering*.

Lu, Z. and Law, S. S. (2006), "Identification of prestress force from measured structural responses", *Mechanical systems and signal processing*, **20,** 2186-2199.

Materazzi, A., Breccolotti, M., Ubertini, F. and Venanzi, I. (2009), "Experimental Modal Analysis for Assessing Prestress Force in PC Bridges: A Sensitivity Study", *Proc. III International Operational Modal Analysis Conference*.

Miyamoto, A., Tei, K., Nakamura, H. and Bull, J. W. (2000), "Behavior of prestressed beam strengthened with external tendons", *Journal of structural Engineering*, **126,** 1033-1044.

Saiidi, M., Douglas, B. and Feng, S. (1994), "Prestress force effect on vibration frequency of concrete bridges", *Journal of structural Engineering*, **120,** 2233-2241.

Wang, L., Hou, J.-L. and Ou, J.-P. (2012), "Moving force identification based on load shape function for a long-span bridge structure", *Chinese Journal of Computational Mechanics*, **29**.

Xu, J. and Sun, Z. (2011), "Prestress force identification for eccentrically prestressed concrete beam from beam vibration response", *Structural Longevity*, **5,** 107-115.

Zhang, Q. (2010). Dynamic load and structural damage identification using virtual distortion method. Ph.D. Dissertation, Harbin Institute of Technology, Harbin.

Zhang, Q., Jankowski, Ł. and Duan, Z. (2008), "Identification of coexistent load and damage based on virtual distortion method", *Proceedings of the 4th European workshop on structural health monitoring, Kraków, Poland*.